Journal of Catalysis **191,** 456–466 (2000)
doi:10.1006/jcat.1999.2791, available online at http://www.idealibrary.com on IDEAL®

Influence of Lanthana on the Nature of Surface Chromium Species in La_2O_3-Modified CrO_x/ZrO_2 Catalysts

A. Trunschke,[1] D. L. Hoang, J. Radnik, and H. Lieske

Institute for Applied Chemistry Berlin-Adlershof, Richard-Willstätter-Strasse 12, D-12489 Berlin, Germany

Received October 15, 1999; revised December 14, 1999; accepted December 14, 1999

Infrared spectroscopy of the adsorbed probe molecules CO, NO, and NH_3, photoelectron spectroscopy, temperature-programmed desorption of NH_3, X-ray diffraction, and BET surface analysis have been used to study surface and bulk characteristics of lanthana-modified CrO_x/ZrO_2 catalysts. La_2O_3 addition to CrO_x/ZrO_2 strongly modifies the structure of supported chromia species and stabilizes coexisting isolated Cr^{3+} and highly dispersed Cr_2O_3 particles. Unlike that, chromia in La_2O_3-free CrO_x/ZrO_2 undergoes considerable sintering at 823 K, which is the necessary reduction and reaction temperature for *n*-octane aromatization, applied as a test reaction. The strong interaction between chromia and La_2O_3-ZrO_2 could be due to an increased number of nonacid hydroxyl groups, which are possibly responsible for a more efficient anchoring of chromia species on the La_2O_3-containing support rather than on pure zirconia. The performances of La_2O_3-promoted and La_2O_3-free CrO_x/ZrO_2 catalysts in *n*-octane aromatization do not differ so dramatically as would be expected from the large differences in the structure of surface chromia species.

Key Words: **chromia catalyst; lanthana-modified zirconia support; *n*-alkane aromatization.**

1. INTRODUCTION

The molecular structure of supported chromium oxide and its relation to catalytic properties has been the subject of considerable interest in academic research, owing to the important status of chromium catalysts in chemical industry. The chromium oxidation and distribution state strongly depend on the Cr loading, the nature of the support, and its surface chemistry (1).

Zirconia-supported chromia catalysts have been thoroughly investigated with respect to the bulk and surface properties and the catalytic performance, especially in hydrogenation/dehydrogenation reactions and aromatization of C_{6+} alkanes (2–13). In comparison with CrO_x/Al_2O_3 catalysts (14, 15), the selectivity to aromatics in the dehydrocyclization of *n*-paraffines can be improved at the expense of cracking products, possibly due to a lower acidity of the zirconia carrier. Moreover, the formation of a Cr_2O_3-Al_2O_3 spinel during catalytic cycling has been discussed as one of the possible reasons for catalyst deactivation in alkane dehydrogenation (16). The unfavorable tendency of zirconia to sinter during calcination is compensated by the effect of chromia to stabilize high surface areas of the catalysts (4, 10). But especially with low chromia loadings, unsatisfactorily poor specific surface areas are obtained. To overcome this disadvantage, zirconia, stabilized by small amounts of lanthanide oxides, can be used as support.

Recently, we have found that chromia supported on lanthana-doped zirconia is able to catalyze the aromatization of C_{6+} alkanes with high selectivity (12). Moreover, we suggested differing catalytic properties of coexisting coordinatively unsaturated Cr^{3+} ions on the one hand and Cr_2O_3 clusters on the other hand by means of ESR spectroscopy (13).

Little is known about the influence of additions of modifying oxides to zirconia on the nature of supported chromia species. The aim of the present work is to elucidate the effect of the modification of zirconia by lanthana on the molecular structure of surface chromium oxide species under reaction conditions of *n*-alkane aromatization. We characterized the bulk structure and morphology of CrO_x/La_2O_3-ZrO_2 catalysts, the oxidation state of chromium, and the chromia distribution on the carrier by XRD, BET, IR spectroscopy, photoelectron spectroscopy, and temperature-programmed desorption of NH_3. The results will be compared with those on the corresponding La_2O_3-free material and will be related to the performances of the catalysts in *n*-octane aromatization.

2. EXPERIMENTAL

Catalysts with varied chromium loading (Table 1) were prepared by impregnating commercial amorphous ZrO_2 or 7 wt% La_2O_3-ZrO_2 (MEL Chemicals, Serial Number XZO 681/01), respectively, with an aqueous solution of

[1] To whom correspondence should be addressed at Institute for Applied Chemistry Berlin-Adlershof, Richard-Willstätter-Strasse 12, D-12489 Berlin, Germany. Fax: +49 30 6392 4370. E-mail: at@aca-berlin.de.

0021-9517/00 $35.00

$(NH_4)_2CrO_4$ at pH 10. The obtained materials were dried at 393 K and calcined in air at 873 K for 4 h. X-ray diffraction patterns of the calcined powders were obtained using monochromatic Cu$K\alpha$ radiation. The catalysts are denominated as $x CrO_x/(La_2O_3$-$)ZrO_2$, where x is the chromium content in weight percent.

Specific surface area and porosity have been determined after calcination of the samples by nitrogen adsorption at 77 K, using a BET surface area analyzer NOVA-1200 (Quantachrome Corporation).

For transmission FTIR spectroscopic studies, self-supporting wafers of the catalysts were placed into an IR cell, allowing thermal treatments in vacuum or in controlled atmospheres. All of the spectra have been normalized with respect to the weight per square millimeter so that the peak intensities became roughly comparable. For DRIFTS measurements, a diffuse reflectance attachment and a modified reaction chamber manufactured by Harrick have been used. The spectra were collected at 313 K on a spectrometer FTS-60 A (Bio-Rad) coadding 256 scans at a resolution of 2 cm^{-1}.

The photoelectron spectra were recorded by a VG ESCALAB 220 iXL spectrometer (VG Instruments) with a Mg$K\alpha$ source and a monochromated Al$K\alpha$ source. For the compensation of charging a flood gun was used with the monochromated source. The binding energy scale was referred to the substrate peaks Zr 3d5 and O1s. Charging effects were below 5 eV. After the satellite substraction at the spectra measured with the nonmonochromated source, the spectra recorded with the nonmonochromated Mg$K\alpha$ and monochromated Al$K\alpha$ radiation show no significant differences for the photoelectron peaks. After vacuum pretreatment or reduction in the pretreatment chamber of the spectrometer, the samples were transferred into the analysis chamber without air contact.

For quantitative analysis, the peak areas were determined using commercial software (17) after the substraction of a Shirley background. The peaks were fitted with Gauss-Lorentz curves. For a better comparability, the peak intensities obtained with this procedure were normalized by division through the transmission function of the spectrometer depending on the emitted electron energy and instrumental parameters and the Scofield factors, which is a theoretically obtained differential cross section for the given shell of the analyzed atom. In the further sections of this papers we will use these normalized peak intensities for a qualitative discussion about the behavior of the Cr species on the different supports. A more quantitative discussion needs a more sophisticated quantitative analysis, which considers more morphological aspects of the catalyst (18).

NH_3-TPD experiments as well as catalytic tests were performed in a characterization apparatus, consisting of a fixed-bed quartz reactor and a gas analysis system. Ammonia has been adsorbed at 373 K. The desorption was performed in a helium flow (15 ml min^{-1}) at a heating rate of 10 K min^{-1}. Aromatization of n-octane was carried out under normal pressure at 823 K. As feed, a hydrogen flow (flow rate = 20 ml min^{-1}) was saturated with n-octane (7.7 kPa). The reaction products were analyzed by an on-line gas chromatograph, equipped with a 50 m PONA capillary column.

3. RESULTS AND DISCUSSION

3.1. Crystal Structure and BET Surface Areas of the Catalysts

It is well known that the addition of small amounts of transition metal oxides to zirconia can change the ZrO_2 phase composition and stabilizes the specific surface area of ZrO_2. According to XRD, amorphous zirconia crystallizes in the monoclinic modification after calcination in air at 873 K (Table 1). La_2O_3-doped zirconia as well as zirconia in the CrO_x/La_2O_3-ZrO_2 catalysts, pretreated at the same temperature, consists almost exclusively of the tetragonal modification. In agreement with the literature (4, 8), chromium in our CrO_x/ZrO_2 catalysts also stabilizes the metastable tetragonal phase. For low chromium loadings (0.5–2 wt%), monoclinic and tetragonal zirconia coexist.

TABLE 1

General Characteristics of the Investigated Catalysts

Support	ZrO_2				La_2O_3-ZrO_2			
Chromium content (wt%)	0	0.5	2	4	0	0.5	2	4
ZrO_2 modification after calcination at 873 K[a]	*m*	*m*	*m*/*t*	*t*	*t*	*t*	*t*	*t*
BET (m^2/g)	33.3	75.3	116.2	136.0	102.0	104.0	130.3	131.3
Total amount of desorbed NH_3 (mmol/g)	0.008	0.036	0.056	0.048	0.100	0.088	0.068	0.080

[a] *m*, monoclinic; *t*, tetragonal.

In catalysts with 4 wt% chromium loading, the tetragonal modification of zirconia predominates.

In Table 1 the specific surface areas of the catalysts after calcination in air at 873 K are summarized. Since zirconia undergoes sintering upon high temperature treatments, the BET surface area of the calcined pure ZrO_2 is rather low. Lanthana exhibits a stabilizing function like chromium in CrO_x/ZrO_2 (4) and prevents sintering of the crystallites during calcination. Thus, the surface area of calcined La_2O_3-ZrO_2 is substantially higher in comparison with calcined pure ZrO_2. The BET surface area of CrO_x/ZrO_2 gradually increases with increasing chromium content and becomes comparable to that of La_2O_3-ZrO_2 at 2 wt% Cr. Hence, the stabilizing effect of lanthana is especially beneficial for low chromium loadings as it becomes evident by the comparison of $0.5CrO_x/ZrO_2$ and $0.5CrO_x/La_2O_3$-ZrO_2. At 4 wt% chromium, the BET values of the lanthana-free and the lanthana-containing catalysts are similar.

Consequently, in order to rule out an influence of varying specific surface areas or changes in the zirconia modification, the discussion of differences in the surface composition of the ZrO_2 and La_2O_3-ZrO_2-supported chromia catalysts will mainly be focused on samples containing 4 wt% chromium.

3.2. Surface Characterization of the Catalysts

The catalyst surfaces have been characterized by infrared spectroscopy, photoelectron spectroscopy, and temperature-programmed desorption of NH_3. At first, the structural features of the supports ZrO_2 and La_2O_3-ZrO_2 will be compared, followed by the discussion of the chromium valence and distribution state in the calcined and reduced chromia catalysts.

3.2.1. Structure of ZrO_2 and La_2O_3-ZrO_2 Supports

Complete dehydroxylation was not observed on the two supports after calcination in air at 873 K followed by vacuum treatment at the same temperature. The higher BET surface area of La_2O_3-ZrO_2 is reflected by an enhanced number of surface OH groups as detected by diffuse reflectance infrared spectroscopy (Fig. 1). ZrO_2 as well as La_2O_3-ZrO_2 exhibits the typical OH bands of isolated terminal and bridged bonded zirconium hydroxyl groups at 3760-55 and 3675-65 cm^{-1}, respectively (19), and a broad feature around 3400 cm^{-1} ascribed to hydrogen-bridged bonded OH groups (20). In contrast to the band at 3760 cm^{-1}, the relative intensities of the bands at 3670 and 3400 cm^{-1} are enhanced by La_2O_3 addition to ZrO_2. This effect can be explained by changes in the structure of the zirconia OH groups due to the presence of lanthana or by a contribution of lanthana hydroxyl group vibrations to the spectrum. Actually, isolated surface La-OH groups have been observed to exhibit a signal at 3660 cm^{-1}

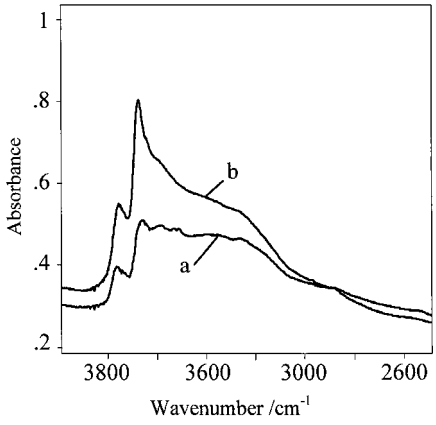

FIG. 1. DRIFT Spectra in the OH stretching region of ZrO_2 (a) and La_2O_3-ZrO_2 (b) after calcination in air at 873 K, followed by vacuum treatment at 873 K.

(21, 22). Peaks near 3585 and 3450 cm^{-1} have been assigned to La(O)OH species (22).

With infrared spectroscopy of adsorbed NH_3, none of these OH groups proved to be able to protonate ammonia, as it is obvious from the absence of signals due to ammonium ions in the spectrum. Only Lewis acid sites have been detected, characterized by bands due to the symmetric and asymmetric deformation vibrations of molecularly coordinated NH_3 at 1180 and 1605 cm^{-1}.

Coordinatively unsaturated sites on the surface of metal oxides are frequently investigated by adsorption of probe molecules, such as carbon monoxide. The infrared spectra of CO adsorbed on ZrO_2 and La_2O_3-ZrO_2 (Fig. 2, a and b) are characterized by a peak near 2200 cm^{-1}. The peak is ascribed to the carbonyl stretching vibration of σ-bonded CO, weakly chemisorbed on coordinatively unsaturated

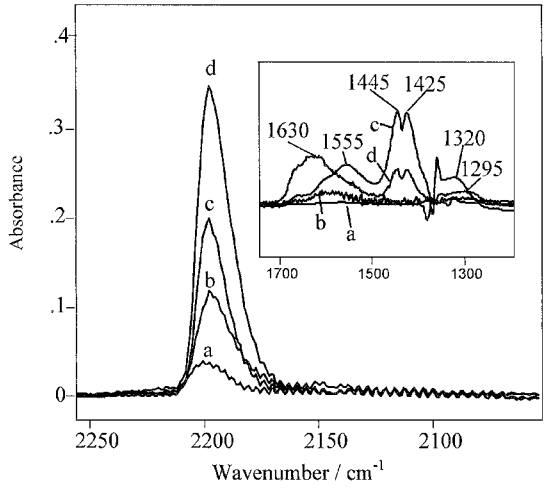

FIG. 2. IR spectra of CO (100 N/m^2), adsorbed at 313 K on ZrO_2 (a), La_2O_3-ZrO_2 (b), $4CrO_x/ZrO_2$ (c), and $4CrO_x/La_2O_3$-ZrO_2 (d) after calcination in air at 873 K, followed by evacuation at 873 K.

(cus) Zr^{4+} ions (23). The higher intensity of the band on La_2O_3-ZrO_2 is related to a higher number of cus Zr^{4+} ions, at first glance due to the increased BET value of this sample. However, the peak area increases to a lesser extent than the surface area, possibly reflecting the partial substitution of zirconium by lanthanum on the surface of the mixed oxide. Lanthanum carbonyls themselves are not expected to be observable, since they are not stable at room temperature (24).

On La_2O_3-ZrO_2, the formation of carbonate species due to reactive chemisorption of CO is observed. These species are characterized by weak bands at 1595 and ca. 1310 cm^{-1} (spectrum b in the inset of Fig. 2). The infrared active ν_3 mode of the C=O stretching vibration in the free carbonate ion is observed near 1400 cm^{-1} (25). Upon coordination of carbonate ions to metal cations, this mode is split into two components. Based on the spectral separation $\Delta\nu(CO) = 285$ cm^{-1} of the two $\nu(CO)$ modes, the former species is assigned to bridged or bidentate carbonates (25). This separation value exceeds reference data $\Delta\nu(CO) = 230$ cm^{-1}, reported in the literature on CO_2 adsorption onto tetragonal zirconia (26). This implies La_2O_3-induced changes in the geometrical configuration of the complexes or the contribution of lanthanum carbonates. In fact, a type of carbonate species similar with regard to the separation $\Delta\nu(CO) = 275$ cm^{-1} and band positions at 1575 and 1300 cm^{-1} has been formed on the surface of La_2O_3 upon CO adsorption at room temperature (24).

To summarize the results of surface characterization of the ZrO_2 and La_2O_3-ZrO_2 supports, the addition of lanthana induces an increase in the number of surface hydroxyl groups. These OH groups exhibit a nonacid character toward ammonia.

3.2.2. *Calcined CrO_x/ZrO_2 and CrO_x/La_2O_3-ZrO_2 Catalysts*

The intensities of the hydroxyl bands observed on the calcined chromium catalysts decrease with increasing chromium content (spectra not shown). With the samples containing 4 wt% Cr, support OH groups are still detectable, indicating that the support surface is not fully covered by oxidized CrO_x species.

The structure of surface chromate species cannot be characterized by IR spectroscopy, due to experimental reasons. The observation range is restricted to 1000 cm^{-1} on the low energy side because of the window material of the infrared cell. However, a band at 1038 cm^{-1} was observed on all samples. The peak has been assigned to Cr=O stretching vibrations of surface chromium oxide species (2, 3, 27, 28).

With ESR investigations previously performed on $4CrO_x/La_2O_3$-ZrO_2 (13), a signal at $g_{II} = 1.959$ and $g_{\perp} = 1.978$ was observed, which was attributed to noninteracting Cr^{5+} ions. Moreover, the presence of isolated Cr^{3+} ions ($g = 4.3$) and Cr_2O_3 clusters ($g = 2$) already in the calcined catalyst, probably formed by thermal decomposition of surface chromates, has been shown.

In the present work, IR spectroscopy of adsorbed CO has been used to study the oxidation state of chromium. Very intense carbonyl peaks are observed upon admission of CO onto the calcined CrO_x catalysts. Figure 2 (c and d) presents the spectra of the samples containing 4 wt% chromium. The peak maxima are slightly red-shifted to 2197 cm^{-1} for $4CrO_x/ZrO_2$ and to 2196 cm^{-1} for $4CrO_x/La_2O_3$-ZrO_2, respectively, compared with the carbonyl spectra on the supports. The interpretation of these spectra is complicated by the fact that the C–O stretching vibration of Cr^{n+} carbonyls ($n = 5$ and/or 4) is located near 2000 cm^{-1} (29). This is also the range, in which Zr^{4+} carbonyls absorb. The latter may be formed on free residual patches of zirconia. However, the intensities of the signals on the chromia catalysts increase with increasing chromium content (Fig. 3). Hence, we conclude that σ-bonded linear Cr^{n+} carbonyls with chromium in high oxidation states ($n = 5$ and/or 4), possibly $Cr^{5+}(CO)$ (29), mainly contribute to the spectrum. Actually, upon subsequent admission of increasing amounts of CO, the growth of the carbonyl band is paralleled by the disappearance of the chromyl band at 1038 cm^{-1}. However, the latter effect may also be due to a shift of this band to the nonobservable range below 1000 cm^{-1}. $Cr^{3+}(CO)$ complexes certainly also contribute to the carbonyl peak near 2200 cm^{-1} (30). The infrared spectra do not contain quantitative information about the abundance of Cr^{6+}, Cr^{5+}, Cr^{4+}, and Cr^{3+} ions on the catalyst surface. The high frequency of the carbonyl peak indicates that mainly carbonyl complexes with chromium ions in high valence states, probably Cr^{5+} and/or Cr^{4+}, are responsible for the spectrum.

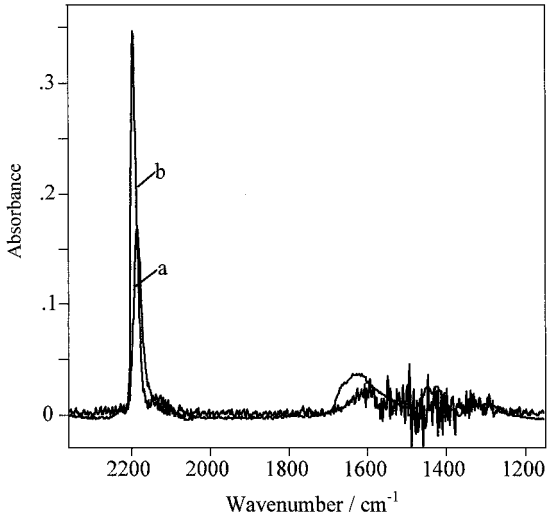

FIG. 3. IR spectra of CO (100 N/m^2), adsorbed on $0.5CrO_x/La_2O_3$-ZrO_2 (a) and $4CrO_x/La_2O_3$-ZrO_2 (b) after calcination in air at 873 K, followed by evacuation at 873 K.

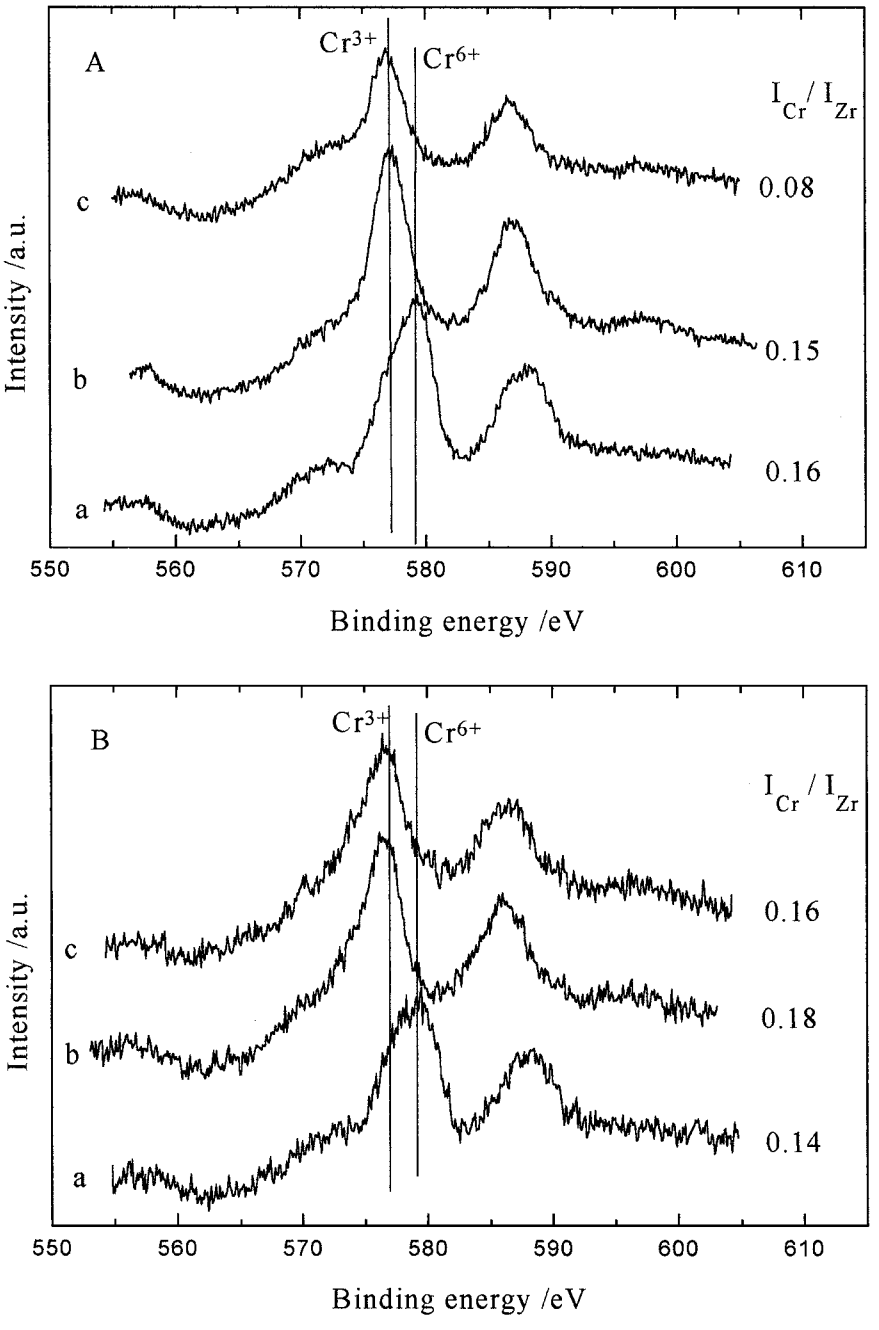

FIG. 4. XPS spectra of $4CrO_x/ZrO_2$ (A) and $4CrO_x/La_2O_3$-ZrO_2 (B) after calcination at 873 K (a) as well as after reduction in hydrogen at 673 K (b) and 773 K (c) for 1 h; intensity ratios between the Cr $2p^-$ and Zr $3d$ peaks are given next to the corresponding spectra.

Further evidence concerning the Cr oxidation state is given by XPS (Fig. 4). The spectra of calcined $4CrO_x/La_2O_3$-ZrO_2 and $4CrO_x/ZrO_2$ show the presence of one peak with a shoulder. The peak, representing a $2p_{3/2}$ binding energy higher than 579 eV, is characteristic for chromium in oxidation state +6. The significant shoulder at lower binding energies is correlated with Cr^{n+} ($3 \leq n \leq 5$).

Infrared spectroscopy of adsorbed CO gave also some information about the distribution state of CrO_x species on the surface of the calcined catalysts. From Fig. 2, it is obvious that the number of cus Cr^{n+} sites ($3 \leq n \leq 5$), giving rise to CO adsorption, is higher on La_2O_3-ZrO_2 than on ZrO_2. Accordingly and keeping in mind that the specific surface areas of the compared CrO_x-containing catalysts are similar, the surface of the La_2O_3-doped zirconia appears to be more capable of spreading chromium species.

The higher coverage of La_2O_3-ZrO_2 by CrO_x species is confirmed by the reactive adsorption of CO that occurs on

the Cr-containing samples to a larger extent than on La_2O_3-ZrO_2. Surface carbonates of a different nature are formed (spectra c and d in the inset of Fig. 2). On $4CrO_x/ZrO_2$, bidentate carbonate complexes, characterized by peaks at 1555 and 1320 cm^{-1}, are observed. The characteristic signals at 1444 and 1425 cm^{-1} have been recently assigned to monodentate carbonates on tetragonal zirconia (26). The carbonate species formed on $4CrO_x/La_2O_3$-ZrO_2 exhibit a band at 1630 cm^{-1} with a shoulder at 1670 cm^{-1} and a peak at 1295 cm^{-1}. The bands at 1630 and 1670 cm^{-1} also appear very weak on $4CrO_x/ZrO_2$. On the basis of literature data, these bands seem to be consistent with the formation of bidentate carbonate complexes on Cr_2O_3 (30). The assignment to chromium carbonate complexes is supported by the fact that the observed species differ from such carbonate-like species, which have been found upon reactive adsorption of CO on La_2O_3-ZrO_2 (Fig. 2 (b)). The lower intensity of the monodentate zirconium carbonate peaks and the higher intensity of the chromium carbonate peaks on $4CrO_x/La_2O_3$-ZrO_2 in comparison with $4CrO_x/ZrO_2$ may imply that less free zirconia surface is available on $4CrO_x/La_2O_3$-ZrO_2. The latter observation also sustains that lanthana addition leads to highly spread chromium oxide species in the calcined catalysts. At first glance, the FTIR results of adsorbed CO conflict with the XPS results, which show a little higher I_{cr}/I_{zr} ratio for the La_2O_3-free zirconia surface than for the La_2O_3-doped surface (Fig. 4). This apparent contradiction can be explained by the different surface sensitivity of the two methods. CO molecules interact only with the outermost surface layer of the sample, so that only the Cr and Zr atoms of these layer are detected by CO-FTIR, while the photoelectrons of the XPS experiments have an inelastic mean free path λ of about 2 nm. Only 10% of the signal comes from the outermost surface layer (18). Consequently, as far as the surface coverage with chromium species is concerned, CO-FTIR is certainly the more reliable method.

Thus it seems that during calcination at 873 K an inhomogeneous CrO_x overlayer is growing on the surface of ZrO_2 or La_2O_3-ZrO_2, respectively, containing chromate and Cr^{3+} species as well as chromium in intermediate oxidation states. Probably, lanthana addition to ZrO_2 induces an increased coverage of the support by chromium species in the calcined samples.

3.2.3. *Reduced CrO_x/ZrO_2 and CrO_x/La_2O_3-ZrO_2 Catalysts*

3.2.3.1. Oxidation and distribution state of chromium. Prereduction in hydrogen at 823 K is essential for the activity of zirconia-supported CrO_x catalysts in *n*-alkane dehydrocyclization, used as a test reaction. The catalytic tests have been performed in hydrogen feed at this high temperature, too. In the following it will be shown that the lanthana-induced high coverage of the support by CrO_x in the calcined sample leads to a higher dispersion of chromium species under these conditions. Here, the term "higher dispersion" comprehends a higher amount of isolated chromium species and/or highly dispersed chromium oxide particles.

Information concerning the near-surface composition as well as the chromium oxidation state has been expected from photoelectron spectroscopy. We applied different reduction temperatures. The corresponding XPS spectra are presented in Fig. 4. Upon reduction at 673 K, a Cr $2p_{3/2}$ binding energy of 577.0 eV has been measured. The signal shifted to 576.0 eV for $4CrO_x/ZrO_2$ and 576.5 eV for $4CrO_x/La_2O_3$-ZrO_2, respectively, when the increased reduction temperature of 773 K was applied. The XPS analysis shows that the higher valent chromium species are converted into three valent chromium during reduction.

Figure 4 also illustrates the changes of the near-surface chromium content in $4CrO_x/ZrO_2$ and $4CrO_x/La_2O_3$-ZrO_2 that have been observed with increasing reduction temperature. The intensity ratios I_{Cr}/I_{Zr} are given next to the corresponding spectra in Fig. 4. With $4CrO_x/La_2O_3$-ZrO_2, the near-surface fraction of chromium detected by XPS remains unaffected or even increases when the reduction temperature is increased. Concerning $4CrO_x/ZrO_2$, a considerable drop of the chromium near-surface concentration has been registered at the highest reduction temperature, most likely due to sintering of chromium species. This result indicates the ability of La_2O_3-doped zirconia to stabilize a high surface concentration of chromium even at high reduction temperatures.

In order to complement the ESCA measurements, adsorption of carbon monoxide was studied by FTIR spectroscopy. In addition to the reduction temperature of 823 K, we applied 673 K, in order to estimate the disturbing influence of Zr^{4+} carbonyls on the spectra of the chromium carbonyls. According to previously performed temperature-programmed reduction studies (31), the reduction of chromium species finishes at about 673 K. The spectra of CO adsorption on $4CrO_x/ZrO_2$ (Fig. 5, a) and $4CrO_x/La_2O_3$-ZrO_2 (Fig. 5, b) after hydrogen pretreatment at this temperature confirm the XPS result that chromium has been completely converted into the valence state +3. In the carbonyl region, the spectra are dominated by a single band at 2187 cm^{-1} on $4CrO_x/ZrO_2$ and at 2182 cm^{-1} on $4CrO_x/La_2O_3$-ZrO_2. The signal is clearly ascribed to the chemisorption of CO on Cr^{3+} (2, 3).

In order to rule out a disturbing influence of Zr^{4+} carbonyl peaks on the spectral features, CO adsorption on the support materials themselves, pretreated under the same conditions, has been performed. A very small peak at 2200 cm^{-1} is observed on ZrO_2 (Fig. 5, c). However, even this small peak could disturb the Cr^{3+}(CO) signal on $4CrO_x/ZrO_2$ to a certain degree, if the essentially larger

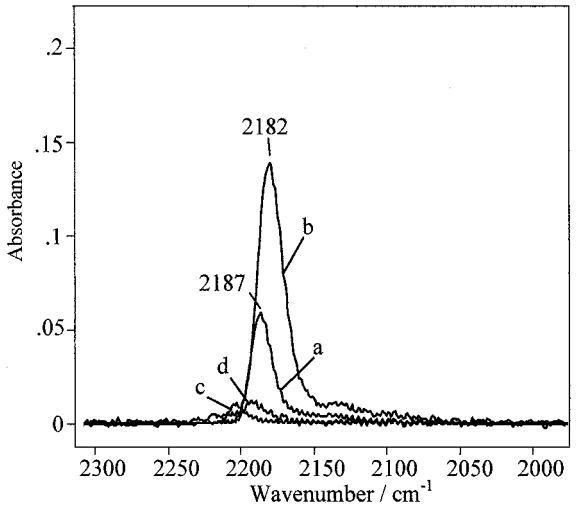

FIG. 5. Adsorption of CO (100 N/m^2) on $4CrO_x/ZrO_2$ (a), $4CrO_x/La_2O_3$-ZrO_2 (b), ZrO_2 (c), and La_2O_3-ZrO_2 (d) after hyrogen pretreatment at 673 K.

BET surface of the latter is considered. Consequently, the slightly increased wavenumber of the Cr^{3+}(CO) signal on $4CrO_x/ZrO_2$ in comparison with $4CrO_x/La_2O_3$-ZrO_2 could be explained by a disturbing influence of the vibrations of zirconium carbonyls formed on chromium-free sections of the catalyst surface. As it is evident from the low intensity of the carbonyl peak in Fig. 5, d, the contribution of Zr^{4+}(CO) to the spectrum of $4CrO_x/La_2O_3$-ZrO_2, in the case that free support surface was available, should be negligible.

In view of the very weak feature around 2135 cm^{-1} in spectrum b, formation of traces of Cr^{2+} on the La_2O_3-doped catalyst cannot be excluded (2, 3). In order to verify the absence of significant amounts of Cr^{2+}, we explored the reduction of the catalyst in CO that is known to lead to a deeper reduction than hydrogen (2). By this treatment, the absorption in the 2150–1900 cm^{-1} range has been significantly enhanced and a broadband near 2135 cm^{-1} has been obtained, indicating the presence of Cr^{2+}.

On the basis of the peak intensities of the Cr^{3+} carbonyl bands shown in Fig. 5 (a and b) and keeping in mind that zirconium carbonyls did not substantially contribute to the spectra, it is deduced that those coordinatively unsaturated Cr^{3+} ions, which are able to coordinate CO, are more abundant on the surface of the La_2O_3-containing sample after reduction at 673 K.

In following experiments, CO adsorption after reduction at 823 K has been performed in order to decide, if the high chromia dispersion is maintained at this high temperature and if oxidation states lower than +3 occur. The spectra are shown in Fig. 6. The absence of strong absorption in the 2150–2000 cm^{-1} range indicates that chromium oxidation states lower than +3 are not formed. This also applies for the reduction in the presence of *n*-octane (spectra not shown).

With $4CrO_x/La_2O_3$-ZrO_2 (Fig. 6A), the chromium carbonyl peak is essentially the same with respect to shape, intensity, and position, after reduction at 673 or 823 K, respectively. Unlike that, on $4CrO_x/ZrO_2$ certain changes in the spectral features are observed with increasing reduction temperature (Fig. 6B). In particular, the carbonyl peak is shifted to 2191 cm^{-1}. Obviously, the contribution of Zr^{4+}(CO) species to the Cr^{3+} carbonyl spectrum is enhanced. A weak shoulder near 2170 cm^{-1} appears at the low energy side of the peak. The shoulder that is only resolved at low CO coverages could be attributed to CO adsorbed on large Cr_2O_3 clusters (30, 32), possibly α-Cr_2O_3, even though it is crystallographically not detectable. The band persists room temperature evacuation for a short time (Fig. 6B), indicating that the Cr^{3+}-CO interaction is strengthened by partial π back-bonding. This observation suggests an increased back-bonding ability of the corresponding

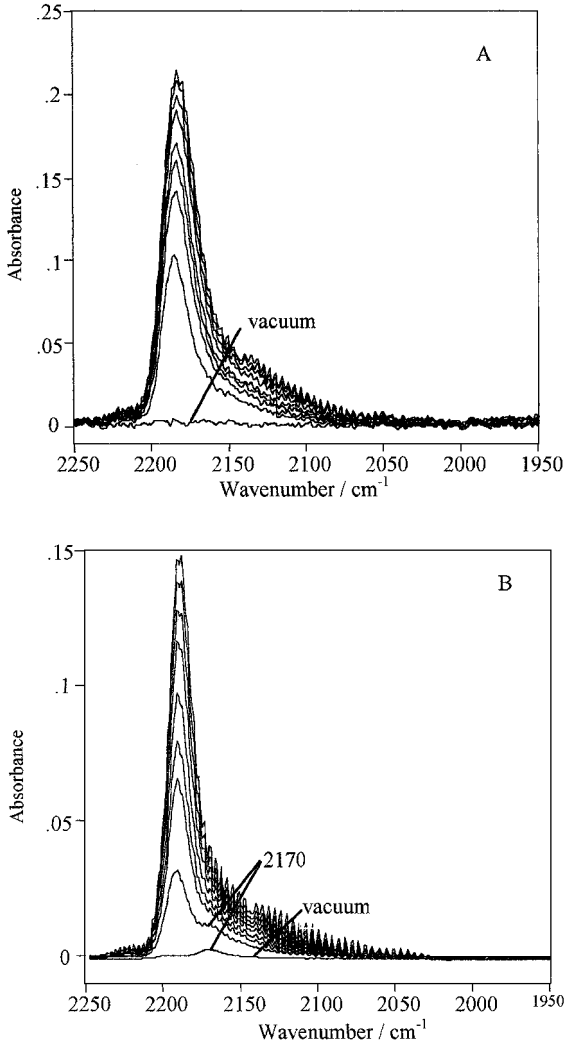

FIG. 6. Adsorption of 10–1000 N/m^2 CO after reduction of $4CrO_x/La_2O_3$-ZrO_2 (A) and $4CrO_x/ZrO_2$ (B) at 823 K.

coordination sites. This is in correspondence with the comparatively low binding energy of chromium $2p_{3/2}$ (576.0 eV) that has been measured by XPS after reduction of $4CrO_x/ZrO_2$ at 773 K (Fig. 4). The very weak peak that remains after evacuation is located at 2170 cm^{-1}. Comparable species are not observed on $4CrO_x/La_2O_3$-ZrO_2, where a higher Cr $2p_{3/2}$ binding energy (576.5 eV) has been measured.

Figure 6 shows the carbonyl spectra in the presence of increasing CO partial pressure. In IR spectroscopic studies of carbon monoxide adsorption on reductively pretreated microcrystalline α-Cr_2O_3, a coverage dependency of the Cr^{3+} carbonyl peak has been observed that has been attributed to adsorbate-adsorbate interactions of the CO molecules, adsorbed in close vicinity on identical coordination sites on flat faces of the α-Cr_2O_3 particles (33, 34). From the intensity of the chromium carbonyl peak on $4CrO_x/La_2O_3$-ZrO_2 (Fig. 6A) and from the coverage independence of its position at 2185 cm^{-1}, we infer that the corresponding adsorption sites may be regarded as isolated Cr^{3+} ions or Cr^{3+} sites located on top of very small, geometrical inhomogeneous, that means amorphous, chromia particles.

Due to the fact that the disturbing influence of Zr^{4+} carbonyls is more pronounced after high temperature pretreatments, the adsorption of CO gave only restricted evidence concerning the chromia distribution state after reduction of the catalysts at 823 K. Especially with $4CrO_x/ZrO_2$ it is not clear if the carbonyl peak is due to Zr^{4+} or Cr^{3+} carbonyl complexes. Therefore, we additionally applied the adsorption of nitrogen monoxide. Mono- and dinitrosylic species of Cr^{3+} and Cr^{2+} ions are expected to appear in the 1900–1650 cm^{-1} region (35). NO selectively probes coordinatively unsaturated chromium ions, because Zr^{4+} merely gives rise to weak, in vacuum instable, mononitrosyls with a band near 1900 cm^{-1}. No evidence was found of NO coordination on the surface of La_2O_3-ZrO_2. Figure 7 compares the infrared spectra after NO adsorption on $4CrO_x/La_2O_3$-ZrO_2 and $4CrO_x/ZrO_2$ previously reduced in hydrogen at 823 K. Upon exposure of $4CrO_x/La_2O_3$-ZrO_2 to NO, an intense doublet at 1852 and 1710 cm^{-1} is observed that corresponds to the symmetric and asymmetric stretching modes, respectively, of dinitrosylic chromium complexes (Fig. 7, a). A mononitrosylic species occurred with a very weak shoulder near 1770 cm^{-1}. The nitrosylic bands exhibit FWHM (full-width at half-maximum) values between 20 and 50 cm^{-1}. This comparatively large range reveals a considerable energetic heterogenity of the chromia species giving rise to NO coordination, which is in accordance with the results of CO adsorption. Similar nitrosyl bands at 1867 and 1737 cm^{-1} appear on $4CrO_x/ZrO_2$ (Fig. 7, b). However, the intensities of these bands are significantly lower than on $4CrO_x/La_2O_3$-ZrO_2. The difference in the intensities of the nitrosyl bands is explained by a higher number

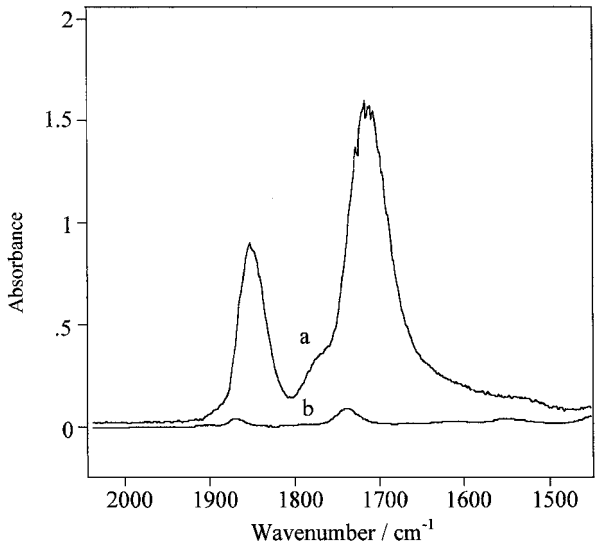

FIG. 7. Adsorption of 100 N/m^2 NO on $4CrO_x/ZrO_2$ (a) and $4CrO_x/La_2O_3$-ZrO_2 (b), followed by evacuation at 313 K.

of coordinatively unsaturated chromium ions, in particular those with two coordination vacancies, on the surface of lanthana-doped zirconia, again indicating the beneficial effect of lanthana on chromia dispersion.

In summary, XPS and infrared spectroscopy of adsorbed CO reveal the dominance of the chromium valence state +3 in the hydrogen and *n*-octane-reduced catalysts, regardless of the support composition. At this point it should be stressed that we have no evidence of the presence of significant amounts of chromium ions in valence states lower than +3. Infrared spectroscopy of the adsorbed probe molecules CO and NO give strong evidence that ZrO_2-supported chromia species are subjected to considerable sintering during reduction at high temperatures. This result corresponds well with the decline of the near-surface chromium concentration observed by XPS after reduction of $4CrO_x/ZrO_2$ at 773 K. Obviously, lanthana-doped ZrO_2 exerts a stabilizing influence on highly dispersed chromia species. This observation is consistent with the results of a recent temperature-programmed reduction study on related catalysts that gave evidence of a stronger interaction between chromia and La_2O_3-ZrO_2 compared with ZrO_2 and a higher part of reoxidable Cr_2O_3 on the surface of La_2O_3-ZrO_2 (31). This stronger interaction could be related to the increased number of nonacid OH groups on the surface of La_2O_3-ZrO_2, as evidenced by infrared spectroscopy (see Section 3.2). The Cr anchorage process can be regarded as an acid-base reaction (1). In fact, the higher OH population surely will contribute to a higher capacity for chromia anchoring and, hence, can be responsible for an enhanced interaction between chromia and the support.

3.2.3.2. Overall acidity of the reduced catalysts. In view of their investigation in *n*-alkane aromatization, the overall

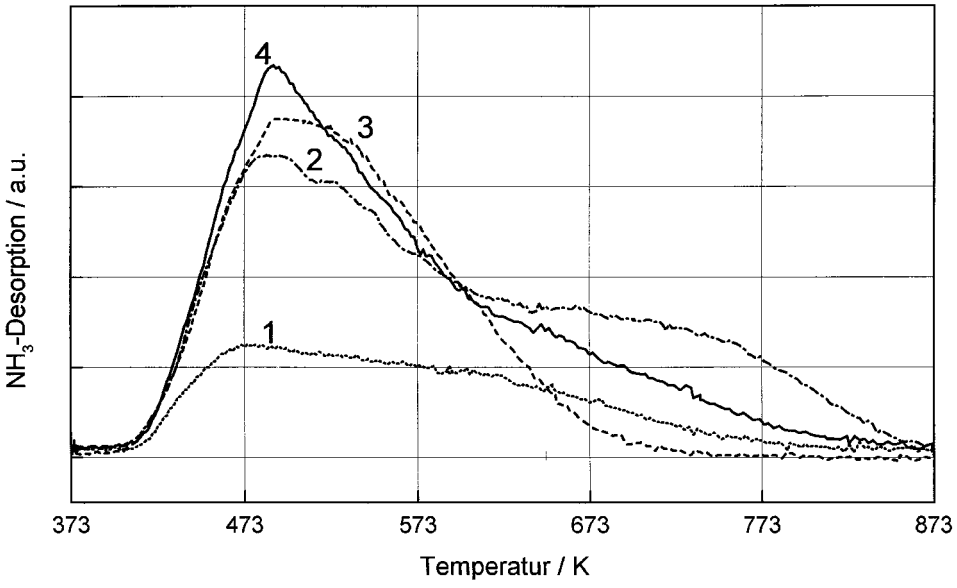

FIG. 8. NH_3 TPD on ZrO_2 (1), 4 CrO_x/ZrO_2 (2), La_2O_3-ZrO_2 (3) and 4 CrO_x/La_2O_3-ZrO_2 (4).

acidity of the reduced catalysts is of interest. Therefore, we have performed temperature-programmed desorption of ammonia.

As mentioned above, the catalysts exhibit only Lewis acid sites as checked by infrared spectroscopy of adsorbed ammonia. In Fig. 8, the results of temperature-programmed NH_3 desorption are shown. The Lewis acidity of all catalysts is low, regarding the number of acid sites (Table 1) as well as their strength. The maxima of NH_3 desorption have been found at temperatures as low as between 473 and 523 K. Sites of such low acidity should not be able to catalyze skeletal conversions of hydrocarbons.

3.3. Performance of the Catalysts in *n*-Octane Dehydrocyclization

The results of *n*-octane aromatization are summarized in Fig. 9. The predominating products are *o*-xylene and ethylbenzene.

ZrO_2 and La_2O_3-ZrO_2 themselves show some catalytic activity. Lanthana moderately changes the catalytic properties of zirconia with respect to selectivity and activity. La_2O_3-ZrO_2 is slightly more active than ZrO_2 due to a somewhat increased cracking activity of the lanthana-containing sample. Considering the larger specific surface area of La_2O_3-ZrO_2, La_2O_3 even seems to inhibit the aromatization.

The addition of chromia promotes the formation of *o*-xylene and ethylbenzene. The lanthana-containing catalysts are always more active than the corresponding La_2O_3-free ZrO_2-supported CrO_x systems. The latter effect is more significant at low chromia loadings, certainly due to the differences in the specific surface areas between the La_2O_3-free and La_2O_3-containing samples.

On the La_2O_3-free and La_2O_3-modified catalysts with 0.5 wt% chromium, comparable selectivities toward aromatics have been observed. With the lanthana-free CrO_x/ZrO_2 samples, the selectivity toward aromatics is almost constant with increasing chromium loading. Unlike the latter, CrO_x/La_2O_3-ZrO_2 samples become more selective in aromatization with increasing chromium loading. As a consequence, the yield of aromatic products is enhanced on the lanthana-promoted samples with higher chromium content (Fig. 9).

3.4. Relations between Catalyst Structure and Performance

According to the surface characterization results, the catalytically active chromium oxidation state in the aromatization of C_{6+} alkanes is doubtless +3. So far, our findings are compatible with conclusions that have been drawn in the literature on the active oxidation state of zirconia-supported chromium catalysts in related catalytic reactions such as dehydrogenation of alkanes and H_2-D_2 equilibration (4, 11). We have no indication that on our catalysts and under our pretreatment and reaction conditions other oxidation states, like Cr^{4+} or Cr^{2+}, are present on the surface of the active catalyst in significant amounts (4, 6).

As it was shown by XPS and infrared spectroscopy, the agglomeration state of the chromia species is completely different on the catalysts compared. La_2O_3-ZrO_2-supported chromia is highly dispersed and exhibits mainly isolated Cr^{3+} ions or coordinatively unsaturated Cr^{3+} ions on top of amorphous Cr_2O_3. Unlike that, Cr_2O_3 supported

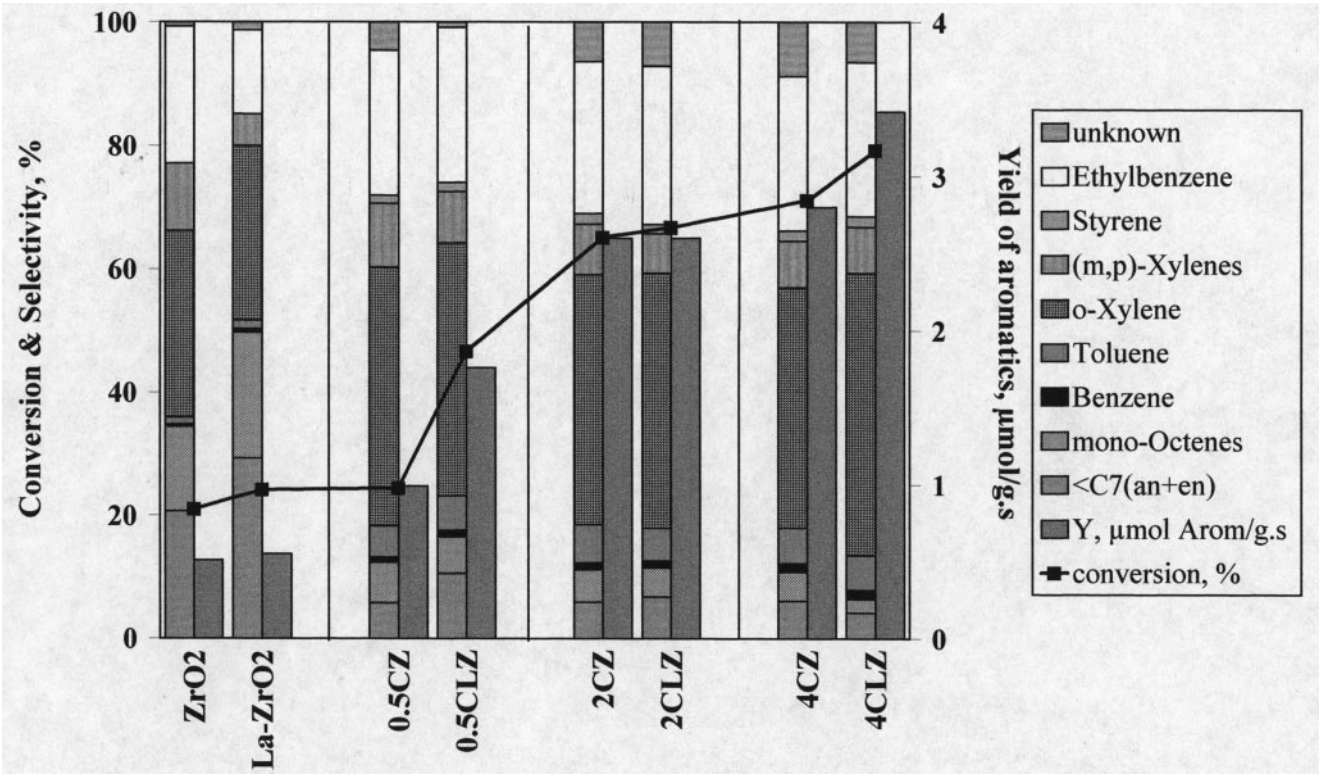

FIG. 9. Aromatization of *n*-octane at 823 K, W/F = 58, analysis after 90 min; CZ, CrO_x/ZrO_2; CLZ, CrO_x/La_2O_3-ZrO_2.

on ZrO_2 substantially sinters, and large chromia particles, possibly α-Cr_2O_3, predominate under reaction conditions. However, the catalytic performances of the two catalysts do not differ so much that we could attribute the catalytic activity to one of the chromia agglomaration states. Therefore, our results rather point to an insensitivity of the aromatization of *n*-alkanes toward the moleculare structure of Cr_2O_3 surface species. Recently, Weckhuysen *et al*. pointed out the importance of both isolated and clustered unsaturated Cr^{3+} centers for the activation of alkanes in dehydrogenation (16). The dehydrogenation of the alkane is assumed to be the first step of the reaction pathway of C_{6+} alkane aromatization, e.g. (36). With the CrO_x/(La_2O_3-)ZrO_2 catalysts a simple product spectrum is observed that is characterized by a predominant formation of ethylbenzene and *o*-xylene. This product spectrum can only be explained by a C_6 ring closure of the *n*-C_8 paraffinic chain. As mentioned, the catalysts exhibit only weak acid sites. On the one hand, this finding explains why the usual by-products of acid-catalyzed side reactions hardly occur in the product spectrum. On the other hand, the inability to catalyze such skeletal conversions should exclude that the C_{6+} ring is formed from a paraffinic or mono-olefinic chain. Therefore, we assume that over CrO_x/(La_2O_3-)ZrO_2 catalysts the aromatization of C_{6+} alkanes proceeds via a stepwise dehydrogenation of the alkane into an alkene, diene, and triene, followed by cyclization, e.g. (37), i.e., according to the so-called triene-mechanism, the cyclization step of which should be less demanding to the catalyst. Therefore, a close relation should exist between alkane dehydrogenation and C_{6+} alkane aromatization activity over ZrO_2-supported chromium catalysts. In so far, our experimental findings support the assumption, given by Weckhuysen *et al*., that isolated as well as clustered Cr^{3+} sites are involved in the dehydrogenation sites. However, further experimental efforts are necessary, especially in order to clarify the catalytic role of the different chromia agglomeration states, especially also with respect to the important problem of catalyst deactivation.

4. CONCLUSIONS

The following conclusions can be drawn:

- We can confirm that lanthana added to zirconia inhibits sintering of zirconia particles and stabilizes the tetragonal modification of zirconia. La_2O_3 ensures high specific surface areas of the CrO_x catalysts also at low chromia loadings. Moreover, the addition of La_2O_3 increases the number of nonacid OH groups on the surface of the support.
- The La_2O_3-modified ZrO_2 support apparently interacts more strongly with chromium species, possibly mediated by a more efficient chromium-anchoring process on these nonacid hydroxyl groups. The strong binding of higher valent chromium species on the surface leads to a stable

molecular distribution of chromium in the calcined catalyst.

- Isolated Cr^{3+} ions and highly dispersed Cr_2O_3 particles are stabilized on the surface of La_2O_3-modified zirconia even during reduction with hydrogen at high temperature, whereas chromia supported on ZrO_2 undergoes considerable sintering.
- Chromia clusters as well as isolated Cr^{3+} centers seem to be active in the C_{6+} aromatization. The high selectivity of the $CrO_x/(La_2O_3\text{-})ZrO_2$ catalysts to aromatics is related to a sufficiently high ability to dehydrogenate the *n*-alkane into mono-olefines and multiunsaturated olefines as well as to the absence of acid-catalyzed side reactions, due to the low overall acidity of these samples.

ACKNOWLEDGMENTS

This work was supported by the Berlin Senat Department of Science, Research, and Culture and by the Federal Ministry of Education and Research of the Federal Republic of Germany. A.T. is grateful for financial support by the Deutsche Forschungsgemeinschaft, Projekt Li 666/4-1. The authors thank BASF AG, Ludwigshaven, Germany, and MEL Chemicals, Manchester, UK, for supporting parts of this work. We thank Dr. M. Schneider for XRD measurements and Mrs. P. Rößler, Mrs. W. Ziesche, and Mrs. K. Weh for technical assistance.

REFERENCES

1. Weckhuysen, B. M., Wachs, I. E., and Schoonheydt, R. A., *Chem. Rev.* **96**, 3327 (1996).
2. Cimino, A., Cordischi, D., Febbraro, S., Gazzoli, D., Indovina, V., Occhiuzzi, M., and Valigi, M., *J. Mol. Catal.* **55**, 23 (1989).
3. Ghiotti, G., Chiorino, A., and Boccuzzi, F., *Surf. Sci.* **251/252**, 1100 (1990).
4. Cimino, A., Cordischi, D., De Rossi, S., Ferraris, G., Gazzoli, D., Indovina, V., Minelli, G., Occhiuzzi, M., and Valigi, M., *J. Catal.* **127**, 744, 761, 777 (1991).
5. De Rossi, S., Ferraris, G., Fremiotti, S., Cimino, A., and Indovina, V., *Appl. Catal. A* **81**, 113 (1992).
6. Arata, K., Hino, M., and Matsuhashi, H., *Appl. Catal. A* **100**, 19 (1993).
7. De Rossi, S., Ferraris, G., Fremiotti, S., Indovina, V., and Cimino, A., *Appl. Catal. A* **106**, 125 (1993).
8. Sohn, J. R., and Ryu, S. G., *Langmuir* **9**, 126 (1993).
9. Ghiotti, G., and Chiorino, A., *Spectrochim. Acta* **49A**, 1345 (1993).
10. Sohn, J. R., Ryu, S. G., and Kim, H. W., *J. Mol. Catal.* **135**, 99 (1998).
11. Indovina, V., *Catal. Today* **41**, 95 (1998).
12. Lieske, H., and Hoang, D. L., German Patent DE-OS 196 12 000.
13. Brückner, A., Radnik, J., Hoang, D.-L., and Lieske, H., *Catal. Lett.* **60**, 183 (1999).
14. Rozengart, M. I., and Kazanski, B. A., *Usp. Khim.* **40**, 1537 (1971).
15. Grünert, W., Saffert, W., Feldhaus, R., and Anders, K., *J. Catal.* **99**, 149 (1986).
16. Weckhuysen, B. M., and Schoonheydt, R. A., *Catal. Today* **51**, 223 (1999).
17. Fison Instrument Eclipse, version 2.01, 1996.
18. Cimino, A., Gazzoli, D., and Valigi, M., *J. Electron. Spectrosc. Relat. Phenom.* **104**, 1 (1999).
19. Tsyganenko, A. A., and Filimonov, V. N., *J. Mol. Struct.* **19**, 579 (1973).
20. Kustov, L. M., *Topics Catal.* **4**, 131 (1997).
21. Lacombe, S., Geantet, C., and Mirodatos, C., *J. Catal.* **151**, 439 (1995).
22. Klingenberg, B., and Vannice, M. A., *Chem. Mater.* **8**, 2755 (1996).
23. Morterra, C., Bolis, V., Fubini, B., and Orio, L., *Surf. Sci.* **251/252**, 540 (1991).
24. Bailes, M., Bordiga, S., Stone, F. S., and Zecchina, A., *J. Chem. Soc. Faraday Trans.* **92**, 4675 (1996).
25. Nakamoto, K., *in* "Infrared and Raman Spectra of Inorganic and Coordination Compounds." Wiley Interscience, New York, 1986.
26. Morterra, C., Cerrato, G., and Ferroni, L., *J. Chem. Soc. Faraday Trans.* **91**, 125 (1995).
27. Vuurman, M. A., Wachs, I. E., Stufkens, D. J., and Oskam, A., *J. Mol. Catal.* **80**, 209 (1993).
28. Weckhuysen, B. M., and Wachs, I. E., *J. Phys. Chem.* **101**, 2793 (1997).
29. Zaki, M. I., and Knözinger, H., *J. Catal.* **119**, 311 (1989).
30. Hadjiivanov, K., and Busca, G., *Langmuir* **10**, 4534 (1994).
31. Hoang, D.-L., and Lieske, H., *Thermochim. Acta*, in press.
32. Scarano, D., Zecchina, A., and Reller, A., *Surf. Sci.* **198**, 11 (1988).
33. Zecchina, A., Coluccia, S., Guglielminotti, E., and Ghiotti, G., *J. Phys. Chem.* **75**, 2774 (1971).
34. Scarano, D., and Zecchina, A., *Spectrochim. Acta* **12**, 1441 (1987).
35. Ghiotti, G., and Chiorino, A., *Spectrochim. Acta* **49A**, 1345 (1993).
36. Paal, Z., *Adv. Catal.* **29**, 273 (1983).
37. Rozengart, M. I., Mortikov, E. S., and Kazansky, B. A., *Dokl. Akad. Nauk SSSR* **166**, 619 (1966).